

Naringenin-7-O-glucoside: Targeting SERPINE1, MMP7, and MMP1 for COVID-19 Lung Pathology and Immune Modulation

Vibha Mishra^{1#}, Shivangi Agrawal^{1#}, Divya¹, Ekta Pathak², Rajeev Mishra^{1*}

Authors share equal contribution

***Corresponding author:**

*Rajeev Mishra, Ph.D.

Bioinformatics Department, MMV
Institute of Science, Banaras Hindu University,
Varanasi-221005, India.

Email: rajeev17@bhu.ac.in; mishrarajeev@gmail.com
Tel: +91 9935338891

¹Bioinformatics Department, MMV, Institute of Science, Banaras Hindu University, India

²Institute of Diabetes and Obesity, Helmholtz Zentrum München, Neuherberg, Germany

Running head: Prunin targets SERPINE1, MMP7, and MMP1

Abstract

The COVID-19 pandemic, caused by the SARS-CoV-2 virus, has been a defining global health crisis, marked by severe respiratory distress and high mortality rates. The search for effective treatments against this highly mutable virus has been a significant challenge. Here, we explored the therapeutic potential of Naringenin-7-O-glucoside (N7G), a bioactive flavone glycoside, in the context of COVID-19. Known for its wide-ranging pharmacological effects, including antiviral, antibacterial, antimalarial, and anticancer properties, Utilizing gene expression data from the EBI Expression Atlas, we analyzed lung samples from deceased COVID-19 patients and healthy individuals to understand N7G's molecular mechanisms and potential therapeutic targets. Our enrichment analysis revealed a significant association of N7G targets with biological functions and pathways crucial in immune responses and cellular signaling. We highlighted the importance of pathways such as HIF-1, AGE-RAGE, and IL-17 in the pathogenesis of diseases like COVID-19. Suppressing the HIF-1 pathway could mitigate lung inflammation, while targeting the AGE-RAGE pathway, a key player in oxidative stress and inflammation, emerges as a promising strategy. Modulating the IL-17 pathway, implicated in cytokine storms during infection, could also be effective. Furthermore, the relaxin signaling pathway, known for its anti-inflammatory and anti-fibrotic properties, was identified as a potential target for post-COVID-19 syndrome or long-haul COVID. We prioritized SERPINE1, MMP7, and MMP1 as key therapeutic targets. Elevated SERPINE1 levels in COVID-19 patients have been linked to early mortality risk and are involved in processes like platelet degranulation and fibrinolysis impairment, contributing to thrombocytopenia. MMP1 and MMP7, part of the matrix metalloproteinases family, play crucial roles in tissue homeostasis and have been identified as biomarkers and potential therapeutic targets in COVID-19, linked to pulmonary edema and severe inflammatory responses. Our molecular docking and MD simulation studies, conducted over 200 ns in triplicates, demonstrated stable complex formation of N7G with MMP7 and SERPINE1. N7G consistently occupied the zinc binding catalytic site of MMP7, similar to other MMP7 inhibitors, and tightly bound to the inhibitor site of SERPINE1, indicating strong interactions. The MMGBSA analysis confirmed the stability of these complexes, suggesting the effective inhibitory potential of N7G against these targets. Although N7G showed transient complex formation with MMP1, its role in COVID-19 pathogenesis, particularly in inflammation, cannot be ignored. Elevated MMP1 levels have been associated with increased inflammatory responses in COVID-19 patients, underscoring its importance as a therapeutic target. In conclusion, our study identifies MMP7, MMP1, and SERPINE1 as critical immune-related targets of N7G in combating COVID-19. The results position N7G as a potential novel inhibitor for treating COVID-19-induced lung inflammation and long-haul COVID. However, these initial findings require further validation. This study contributes to the understanding of natural compounds in viral infection treatment, opening pathways for exploring flavonoids like N7G against SARS-CoV-2 and other viruses. It underscores the importance of diverse therapeutic strategies, including natural substances, in combating the global challenge of COVID-19.

Keywords: Naringenin-7-O-glucoside, COVID-19, long-haul COVID, Multi-target, Matrix Metalloproteinases, Serpin family E member 1 (SERPINE1), Network Pharmacology, Molecular Docking, Molecular Dynamics Simulation

Introduction

The COVID-19 pandemic, caused by the severe acute respiratory syndrome coronavirus 2 (SARS-CoV-2), has significantly impacted global health. Characterized by symptoms such as acute respiratory distress syndrome, it is often linked with host immunological dysfunction and lymphopenia [1-4]. This association leads to increased mortality and adverse outcomes in multiple organ systems among hospitalized patients. The risk of death and hospital readmission remains high for COVID-19 patients, even up to six months post-infection. The burden of COVID-19 extends beyond the acute phase of illness, with considerable health loss observed in the post-acute phase [5, 6]. This underscores the need for effective strategies to reduce infection risk and hospital admissions, as well as the development of post-acute care approaches to mitigate long-term health impacts. Developing therapeutic drugs for COVID-19 poses a challenge due to the virus's high mutagenic and resistance potential [7-10], highlighting the need for pharmacological interventions that are effective in modulating the host's immune response.

Naringenin-7-O-glucoside (N7G), colloquially termed Prunin, is a glycosylated flavonoid prevalent in various citrus fruits, including grapefruits and oranges, as well as tomatoes [11]. N7G has garnered attention due to its broad pharmacological spectrum, offering cardioprotective [12, 13], antioxidant [12, 14-16], anti-diabetic [17-19], anti-hyperlipidemic [17, 20], hepatoprotective [21], anti-bacterial [14], anti-inflammatory [15], anti-apoptotic, and anti-viral benefits [22, 23]. Additionally, N7G's implications for neurological health suggest benefits in managing neurodegenerative diseases and maintaining endothelial cell function. These properties highlight Prunin's potential for integration into pharmacological and nutritional interventions. Its place within the flavonoid O-glycosides class underscores its importance in both natural medicine and various industries. The substance's biomedical relevance is accentuated by its ability to modulate multiple signaling pathways, including Erk1/2 and PI3/Akt, and directly activate PPAR γ , influencing vital cellular processes [17]. Prunin's therapeutic efficacy is evidenced through its interaction with molecular targets such as protein tyrosine phosphatase 1B (PTP1B) and α -glucosidase [18], and its specific binding with viral proteins, suggesting a role in combating viral pathogens like the Marburg virus and SARS-CoV-2 [24, 25]. Given its versatile bioactivity, N7G is recognized as a potent candidate in the management of metabolic and disease processes. Its

demonstrated efficacy through scientific research supports its standing as a promising bioactive therapeutic agent.

In this study, we aim to investigate the potential of Naringenin-7-O-glucoside (N7G) as a therapeutic agent against SARS-CoV-2, focusing on its effects on lung tissue. Utilizing lung samples from both deceased and healthy patients, we explore the interaction of N7G with key gene targets. Our approach combines gene expression data, biological functions and pathway enrichment, network pharmacology, molecular docking and molecular dynamics simulation to elucidate the mechanisms underlying N7G's therapeutic potential. The findings of this study are expected to provide valuable insights into the role of N7G in modulating immune responses and gene expressions in lung diseases, potentially offering a new avenue for treatment strategies against SARS-CoV-2 and similar pathologies.

Materials and Methods

Identification of N7G Targets

First, we predicted the gene targets of N7G using SwissTargetPrediction and SEA [26, 27]. We then analyzed RNA-seq data from the lungs of deceased SARS-CoV-2 patients versus healthy controls, utilizing the Expression Atlas database [28, 29] and identified the differentially expressed gene targets of N7G. We compared and visualized the overlapping genes using the Venny 2.0 online tool (<http://bioinfogp.cnb.csic.es/tools/venny/>).

Protein-Protein Interaction Network and Module Identification

The Protein-Protein Interaction Network for N7G targets was established by integrating data from STRING into Cytoscape, including 100 related proteins based on a minimum confidence score of 0.4. Functionally relevant clusters within this network were detected using the MCODE algorithm, with specific criteria for the degree of association within these modules [30].

Enrichment Analysis for Biological Functions and Pathways

Subsequent enrichment analyses were conducted to discern the biological functions and pathways associated with the network modules [31, 32]. This was achieved through the Enrichr and KEGG databases, identifying the most statistically significant biological processes,

molecular functions, cellular components, and pathways, visualized with the ggplot2 package [33].

Identification of Respiratory Tract Related Disease Terms

The disease enrichment analysis was performed using the Enrichr database [31], followed by identification of respiratory tract related pathologies/ disorders associated to SERPINE1, MMP7 and MMP1 using DisGeNET (<https://www.disgenet.org/>). The cut-off criteria to identify the statistically significant results were set to adjusted p-value < 0.05.

Molecular Docking of N7G with Host Targets

To explore the binding interactions of N7G (Chemical ID: 24211954) with relevant host proteins, we utilized AutoDock Vina 1.2.0 [34], setting an exhaustiveness level of 200 for precision. The three-dimensional protein structures of matrix metalloproteinase MMP7 (PDB: 2Y6D), MMP1 (PDB: 1SU3), and SERPINE1 (PDB: 1A7C) were downloaded from protein data bank [35], and prepared for docking using AutoDock tools [36]. The docking grid parameters were defined with 1Å spacing, based on the binding sites of co-crystallized reference compounds to ensure accurate positioning. Post-docking, we employed UCSF Chimera for 3D interaction analysis [37] and Maestro-12.4.4 (Schrödinger Release 2020–2: Maestro, Schrödinger, LLC, New York, NY, USA) for detailed 2D interaction profiles, comparing N7G's binding affinities to those of reference ligands.

Validation of N7G Binding Affinity

The stability of the N7G molecule in complex with SERPINE1, MMP7, and MMP1 was confirmed through 200 ns molecular dynamics (MD) simulations conducted using GROMACS software version 2021.1, and guided by the CHARMM 36m force field [38, 39]. To ensure reliability, these simulations were performed in triplicates. SwissParam provided the necessary parameters for the ligand, including topology and atomic charges [40]. Our simulation environment was a triclinic water box using TIP3P water, supplemented with sodium and chloride ions to achieve charge neutrality. Following the initial energy minimization and system equilibration, the MD simulations were performed, maintaining a constant 300 K temperature and 1 bar pressure, controlled by the V-rescale thermostat and Parrinello-Rahman barostat [41,

42]. To calculate electrostatic forces and maintain bond lengths, we employed the Particle Mesh Ewald method [43] and LINCS algorithm [44], respectively.

Our simulations tracked the system's evolution by recording the coordinates at 10 ps intervals, totaling 20,000 frames. Analysis of these MD trajectories was conducted through root mean square deviation (RMSD) of the protein backbone, indicating the conformational stability over time; radius of gyration (Rg), which measures the compactness of the complex; details the minimum distance metrics between N7G and MMP7, the hydrogen bonds formed during the simulation; the Solvent Accessible Surface Area (SASA), relating to the exposure of the complex to solvent; and the Root Mean Square Fluctuations (RMSF) of residues close to the ligand (within 5 Angstroms). Plot generation was performed with XMGRACE software (<https://plasma-gate.weizmann.ac.il/Grace/>).

For detailed interaction assessment, we focused on the most representative cluster snapshot, visualized with UCSF Chimera [37], and performed two-dimensional interaction analysis using Maestro Maestro-12.4 4 (Schrödinger Release 2020–2: Maestro, Schrödinger, LLC, New York, NY, USA).

Free energy calculations

From the dataset of the 200 ns molecular dynamics (MD) simulation, we selected a subset of 400 snapshots, ranging from frame 18000 to 20000 and spaced by every 5th snapshot, to calculate the free energy using the Molecular Mechanics Generalized Born Surface Area (MMGBSA) method. These calculations were executed using the MMPBSA.py [45-47]. Additionally, we performed a residue energy decomposition analysis to ascertain the contribution of each amino acid residue to the overall energy of the system. Residues energy decomposition analysis was also performed to evaluate the energy contribution of each amino acid residue to the total energy. For free energy calculation, the following equation was used:

$$\Delta G (\text{bind}) = \Delta G (\text{complex}) - [\Delta G (\text{receptor}) + \Delta G (\text{ligand})]$$

The binding free energy (ΔG_{Total}) was estimated using van der Waals energy (ΔE_{VDW}); electrostatic energy (ΔE_{EEL}); polar solvation energy (ΔE_{GB}); non-polar solvation energy (ΔE_{Surf}); total solvation free energy (ΔG_{Sol}); total gas-phase free energy (ΔG_{gas}).

Results

Identification of Naringenin-7-O-glucoside gene targets

We predicted 128 targets of Naringenin-7-O-glucoside (N7G) and compared them against the significantly upregulated genes obtained from the RNAseq data analysis of lung samples obtained from nine patients who died of COVID-19 [28, 29]. We found 17 significantly upregulated gene targets of N7G. These targets include AKR1B10, ALDH1B1, AMPD3, CA1, CA12, CASP7, CYP19A1, CYP1B1, LDHA, MMP1, MMP7, MMP8, MMP12, PIM2, PLA2G2A, SERPINE1 and YARS1 genes (Figure 1). Further, by mapping the transcript counts of the genes, we validated the upregulation of these gene targets. Out of all the 17 N7G targets, the expression of the SERPINE1 gene was highest followed by LDHA, CYP1B1, PLA2G2A, MMP12, and others (Figure 1).

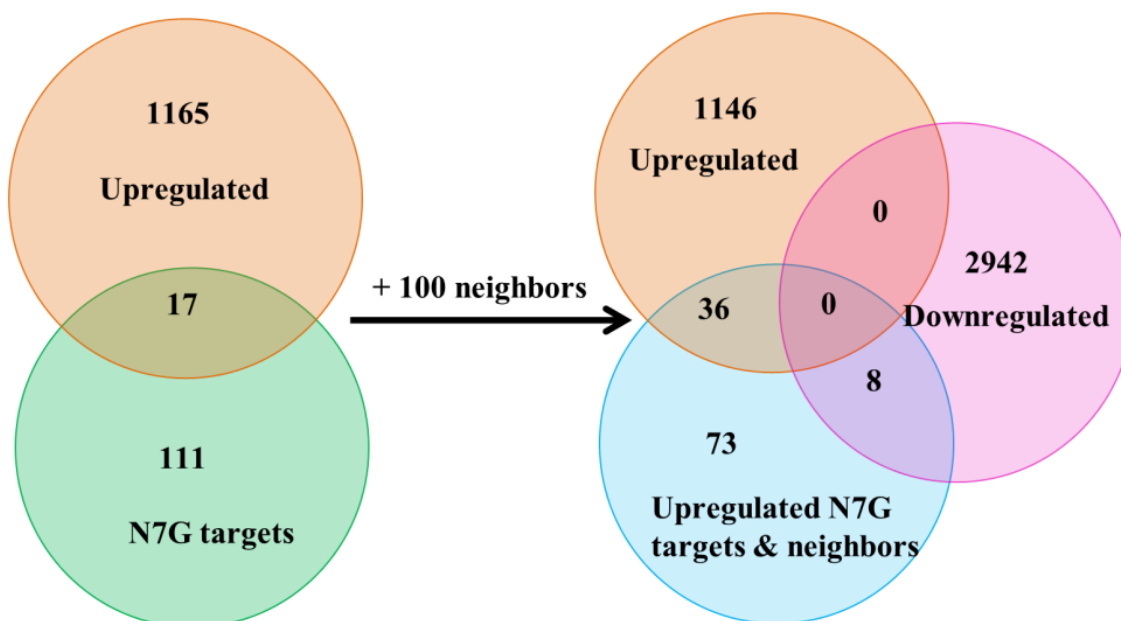


Figure 1: N7G Targets in Lung Cells. (A) Venn diagram indicating overlap of predicted N7G targets and differentially expressed neighboring genes.

Biological significance of the N7G targets

PPI network was constructed for the 17 N7G targets along with 19 upregulated and eight downregulated neighbors. The network consisted of 44 nodes and 307 edges (Figure 2). Next, we identified a module network in the PPI network consisting of 19 nodes and 156 edges and an MCODE score = 17.333. The upregulated N7G targets including MMP1, MMP7 and SERPINE1 formed the part of the module network (Figure 2).

The enrichment analysis of the module revealed biological process such as extracellular matrix organization, external encapsulating structure organization, extracellular structure organization, cellular response to cytokine stimulus, regulation of angiogenesis and platelet degranulation. The enriched molecular functions containing N7G targets include metalloendopeptidase activity, endopeptidase inhibitor activity and protease binding as some of the most significant functions. Similarly, the cellular component analysis revealed the association of N7G targets with terms i.e., platelet alpha granule lumen, platelet alpha granule and collagen-containing extracellular matrix (Figure 3).

Further, the pathway enrichment revealed that the module network was mainly involved in immune related and signaling pathways. On analysing the significant KEGG terms we obtained nine pathways wherein N7G targets are included (Figure 3A). These KEGG terms include HIF-1 signaling pathway, AGE-RAGE signaling pathway in diabetic complications, pathways in cancer, rheumatoid arthritis, IL-17 signaling pathway, bladder cancer, p53 signaling pathway, lipid and atherosclerosis, and relaxin signaling pathway (Figure 3B).

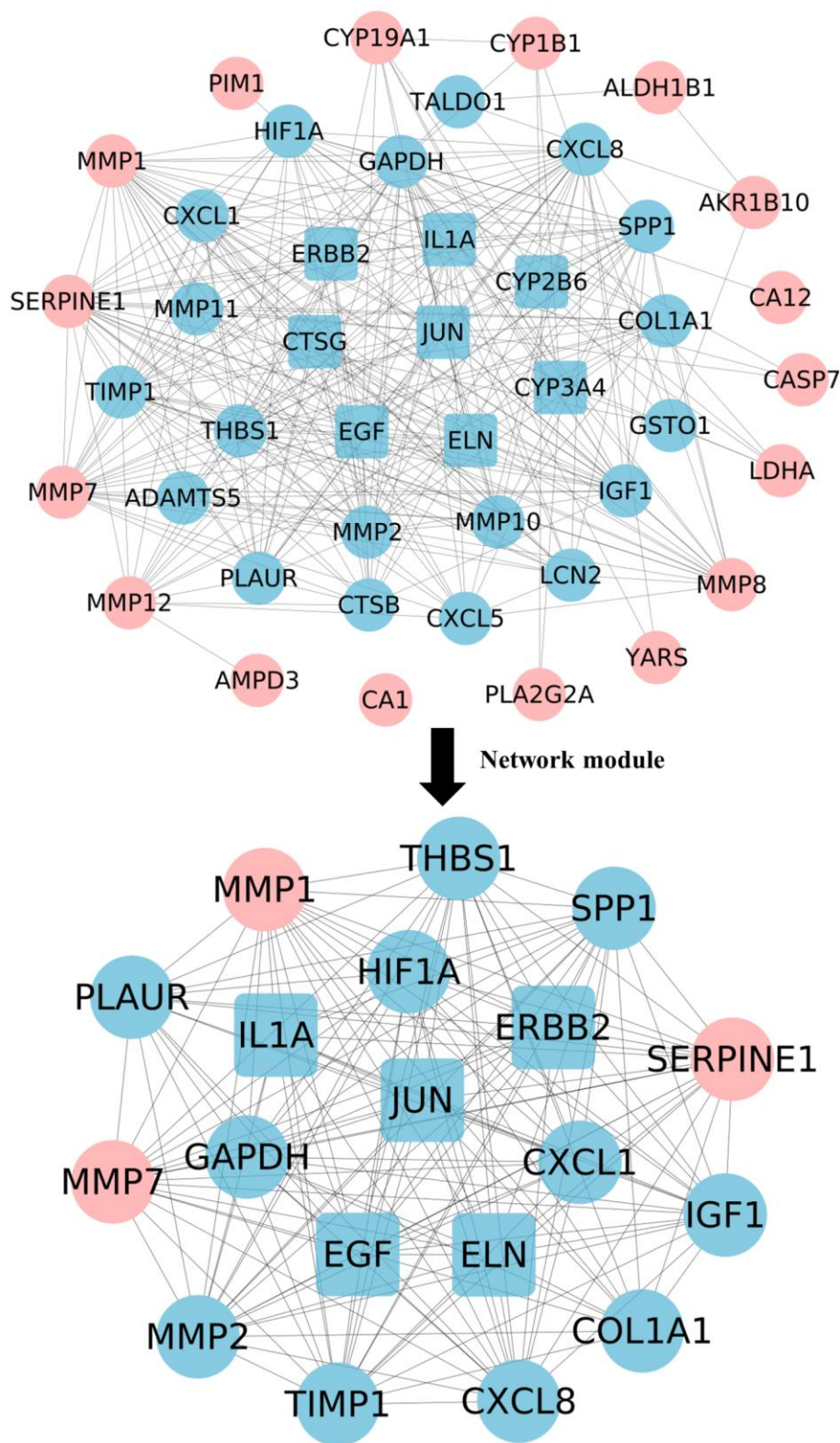


Figure 2: Interaction Network of N7G Targets in Lung Cells. Protein-Protein Interaction (PPI) and network modules showing interactions of dysregulated N7G targets (peach circles) with upregulated (blue circles) and downregulated (blue squares) neighboring genes.

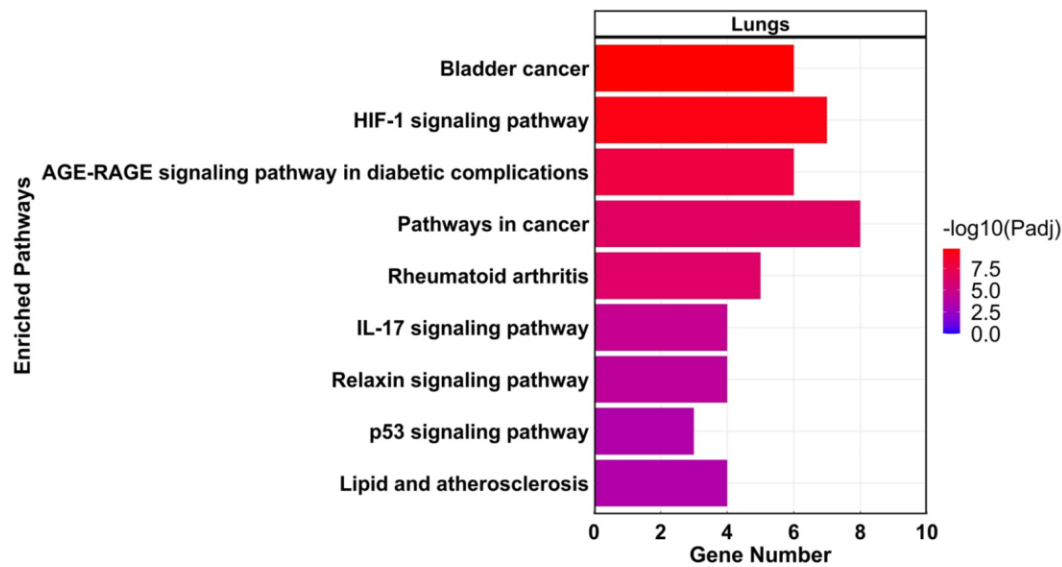
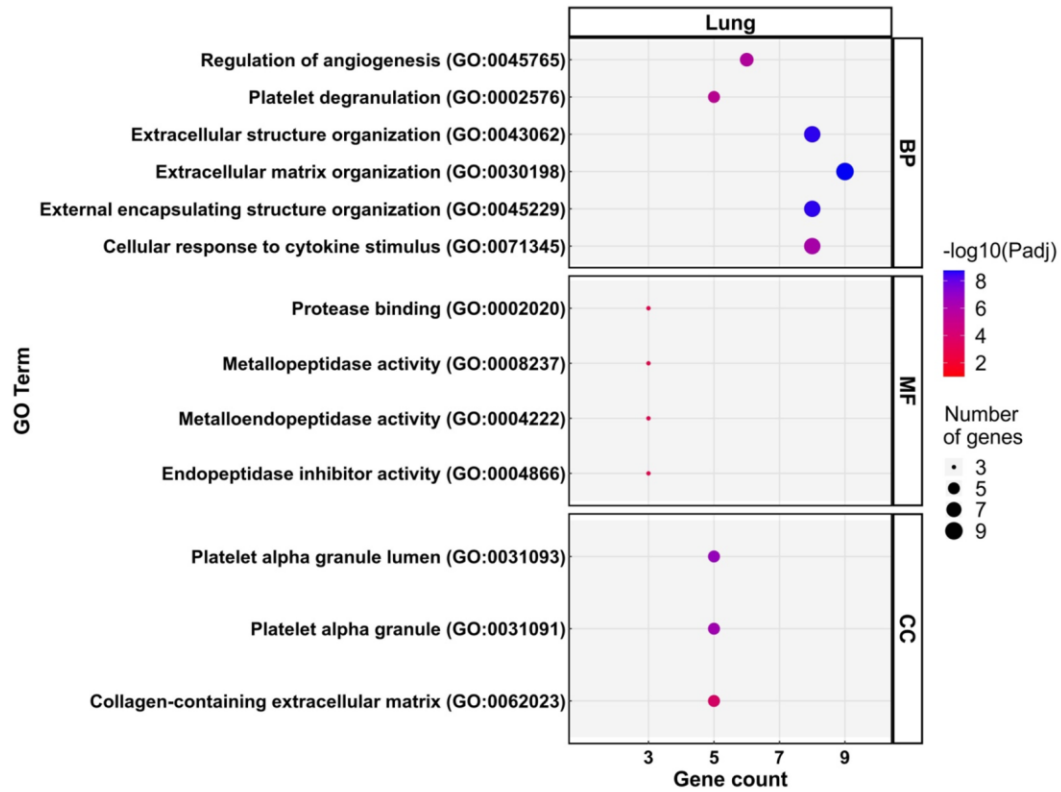


Figure 3: Enrichment Analysis of Module network. Enrichment analysis highlighting the top significant biological processes (BP), cellular components (CC), and molecular functions (MF) related to N7G targets, marked with red stars. (D) Bar plot of significantly enriched pathways within the module network linked to N7G targets.

Identification of Key Respiratory Disorders Linked to N7G Targets

Our disease enrichment analysis, has identified statistically significant associations between N7G targets (SERPINE1, MMP7, and MMP1) and various respiratory tract diseases. The analysis yielded low adjusted p-values, denoting these associations are statistically robust. Idiopathic Pulmonary Fibrosis and Lung diseases shared the most significant association with our gene targets (adjusted P-value: 3.05E-04), while conditions like Asthma also showed significant associations (adjusted P-value: 0.002013276). These findings suggest a potential link between N7G gene targets and the pathogenesis of diverse pulmonary conditions (Figure 4 & Table 1).

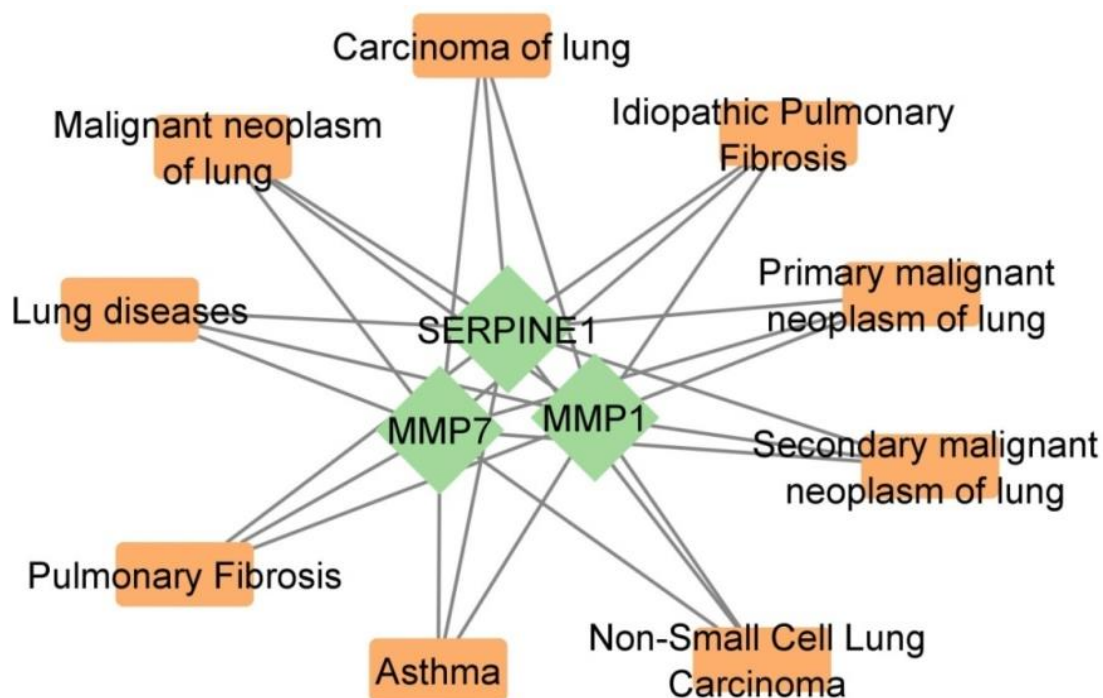


Figure 4: Respiratory Disorders Linked to N7G Targets SERPINE1, MMP7, and MMP1.

Table 1. Respiratory Disorders Linked to N7G Targets

Respiratory Tract Disease Terms	DisGeNet Disease Id	P-value	Adjusted P-value
Secondary malignant neoplasm of lung	C0153676	3.97E-05	7.04E-04
Pulmonary Fibrosis	C0034069	1.00E-05	3.82E-04
Idiopathic Pulmonary Fibrosis	C1800706	6.75E-06	3.05E-04
Lung diseases	C0024115	7.53E-06	3.05E-04
Carcinoma of lung	C0684249	0.001895364	0.006514246
Malignant neoplasm of lung	C0242379	0.001834007	0.006360671
Primary malignant neoplasm of lung	C1306460	0.001456535	0.00571981
Non-Small Cell Lung Carcinoma	C0007131	0.001408877	0.005657752
Asthma	C0004096	2.82E-04	0.002013276

Molecular Docking of N7G with MMP7, SERPINE1, and MMP1

The molecular docking analysis provided insight into the binding affinities of N7G with target proteins, revealing the formation of stable complexes with MMP7, SERPINE1, and MMP1. Binding energies were determined to be -9.5 kcal/mol for MMP7, -9.1 kcal/mol for SERPINE1, and -8.4 kcal/mol for MMP1, indicating strong interactions, particularly with MMP7 and MMP1 which showed higher binding energies than those of their respective reference compounds. SERPINE1's binding energy was found to be comparable to that of its reference compound, as listed in Table 2.

Protein-ligand interaction profiles showed that N7G occupied the active sites of these proteins in a manner similar to their respective reference ligands, as demonstrated in Figure 5. Detailed 2D interaction analysis for the MMP7-N7G complex revealed several non-polar interactions with key amino acid residues. Additionally, the formation of hydrogen bonds with Pro233, Asn234, and Ala235 played a significant role in stabilizing the complex (Figure 5).

In the SERPINE1-N7G complex, the binding was predominantly due to non-polar interactions with hydrophobic residues, complemented by polar interactions and hydrogen bonding with Asn167, among others. The positively charged interactions with residues such as Lys323 and Lys325 further contributed to the stability of the complex.

Analysis of the MMP1-N7G complex highlighted a combination of non-polar and polar interactions, with additional contributions from charged residues, leading to robust binding within the active pocket of MMP1. N7G was also observed to form hydrogen bonds with Arg208 and Phe242.

Table 2: Molecular Docking of N7G with MMP7, SERPINE1, and MMP1

N7G Target (PDB ID)	Reference Ligand	Binding Affinity (Kcal/mol) Reference ligand	Grid box Center	Grid box Size	Binding Affinity (Kcal/mol) N7G
MMP7 (2Y6D)	N-[(2S)-1-[4-(5-Bromopyridin-2-yl)piperazin-1-yl]sulfonyl-5-pyrimidin-2-yl-pentan-2-yl]-n-hydroxy-methanamide	-7.9	x= -18.187 y= 10.426 z= 04.244	x= 24 y= 32 z= 22	-9.5
SERPINE1 (1A7C)	Pentapeptide	-10.0	x= 17.565 y= 20.457 z= 17.224	x= 34 y= 28 z= 60	-9.1
MMP1 (1SU3)	Q27451041	-6.7	x= 49.048 y= -29.726 z= 61.038	x= 30 y= 36 z= 26	-8.4

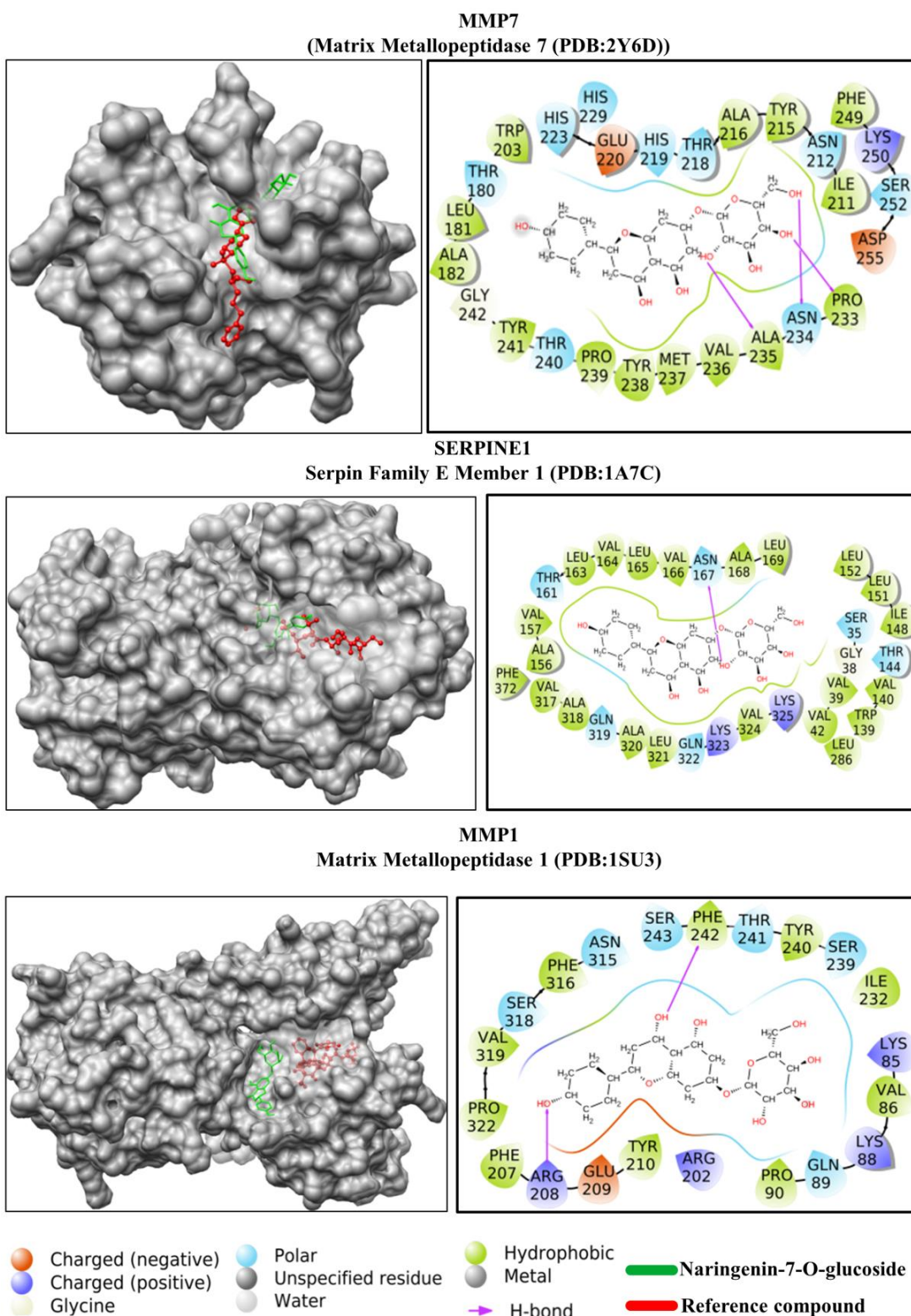


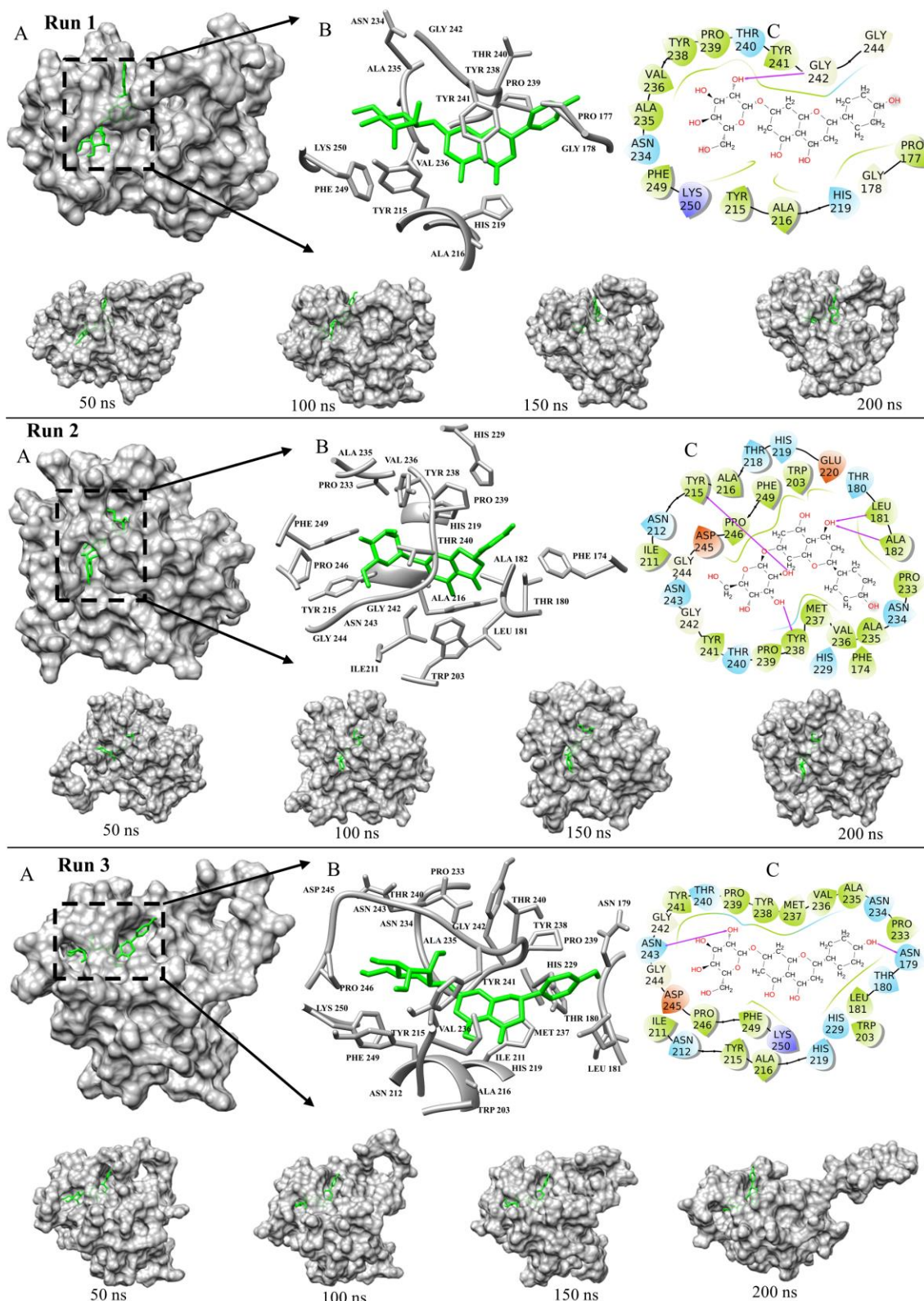
Figure 5: N7G binds to host MMP7, SERPINE1, and MMP1. Surface and 2D interaction views of N7G in complex with cellular targets, compared with reference molecules.

Molecular Dynamics Insight into the MMP7-N7G Binding Mechanism

The binding of N7G to MMP7 was corroborated through extensive molecular dynamics (MD) simulations, performed over 200 nanoseconds in triplicate. The occupation of N7G at MMP7's zinc binding catalytic site was consistent with that of its established inhibitors [48, 49]. N7G displayed numerous non-polar interactions with the hydrophobic residues within MMP7's pocket, namely Tyr215, Ala216, Ala235, Val236, Tyr238, Pro239, and Phe249, maintaining consistency across all trajectory analyses. Hydrophilic interactions were noted with His219, Asn234, and Thr240, alongside charged interactions with Lys250, Glu220, and Asp245. The formation of one to four hydrogen bonds between N7G and MMP7 was observed, contributing to the stability of the complex, as evidenced in Figure 6.

The MMP7-N7G complex exhibited stable backbone conformations, with an average root-mean-square deviation (RMSD) of 0.4 ± 0.01 nm in the first and second runs. A slight fluctuation was noted in the third run, as shown in Figure 7A. N7G maintained a stable RMSD of 0.5 ± 0.1 nm throughout all simulations (Figure 7B). The proximity of N7G within MMP7's active site was indicated by an average minimum distance of 0.18 nm (Figure 7C). Additionally, the radius of gyration (R_g) values remained stable at 1.6 ± 0.03 nm in the first two runs, with minimal fluctuation observed in the third, suggesting a compact and stable complex (Figure 7D). The complex stability was further supported by an average of five hydrogen bonds throughout the triplicate simulations (Figure 7E). The solvent accessible surface area (SASA) demonstrated consistency in the triplicate runs (Figure 7F), and the root-mean-square fluctuation (RMSF) analysis showed minimal fluctuations of catalytic residues, which were effectively shielded by N7G (Figure 7G).

The MMGBSA calculations supported these findings, yielding binding free energies of -41.5428 ± 4.7443 kcal/mol, -46.1620 ± 4.0393 kcal/mol, and -34.2582 ± 3.7192 kcal/mol across the three runs (Table 3). The residue decomposition analysis identified key contributors to the stabilization of the MMP7-N7G complex, with significant energy contributions from Tyr215, Tyr241, Ala235, Tyr238, Val236, Pro239, Ala216, Thr240, Leu181, Ile211, Phe249, Met237, His219, Asn234, and Gly242 as highlighted in Figure 7H. Additional residues with smaller energy contributions are detailed in Figure 7H.



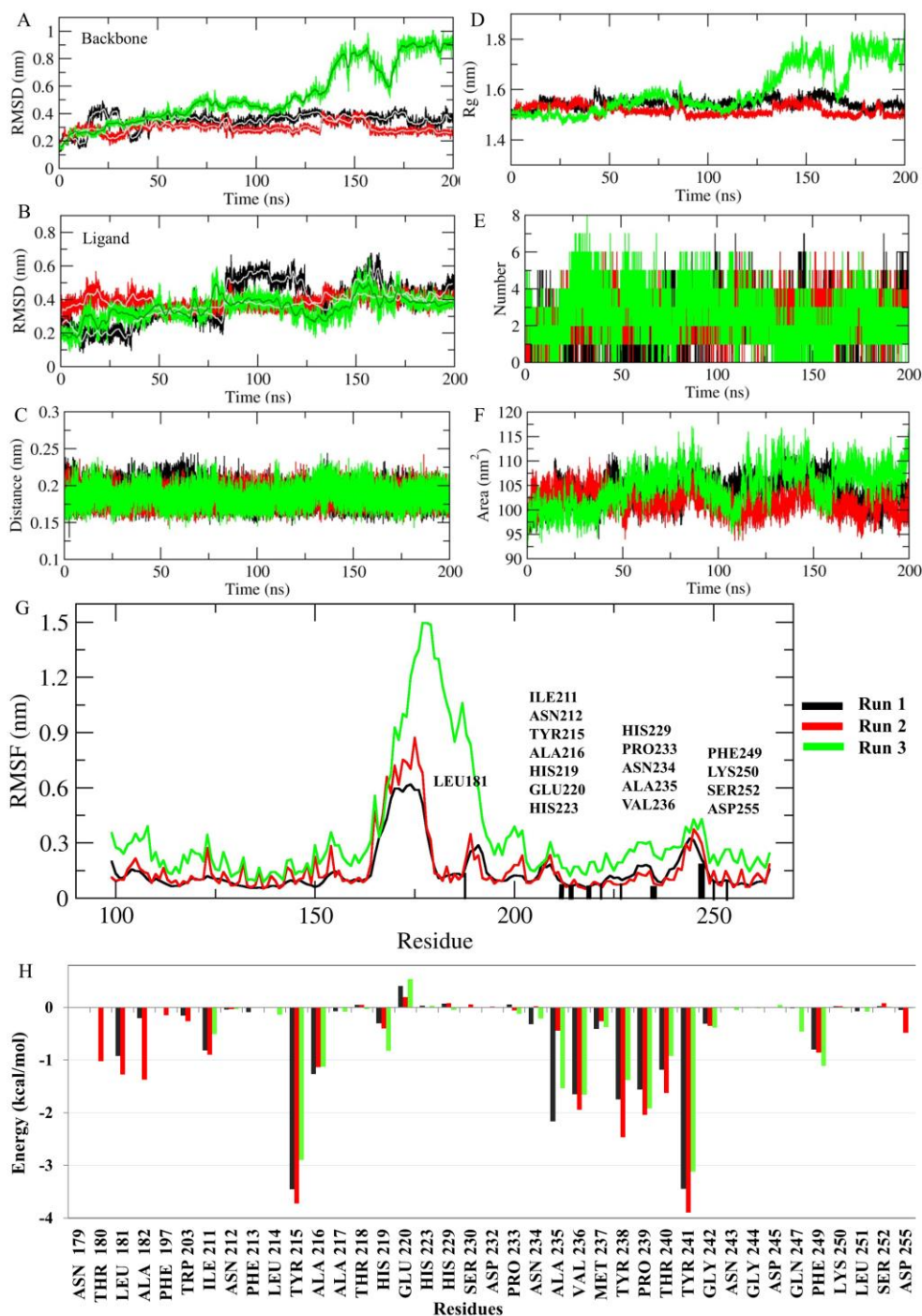


Figure 7: Stability Analysis of the MMP7-N7G Complex via Molecular Dynamics Simulations. (A) the root mean square deviation (RMSD) of the protein backbone, indicating the conformational stability over time; (B) RMSD of N7G within the binding site, reflecting the steadiness of ligand positioning; (C) presents the radius of gyration, which measures the compactness of the complex; (D) details the minimum distance metrics between N7G and MMP7, a direct indicator of binding proximity; (E) enumerates the hydrogen bonds formed during the simulation, a key factor in complex stability; (F) depicts the Solvent Accessible Surface Area (SASA), relating to the exposure of the complex to solvent; and (G) provides the Root Mean Square Fluctuations (RMSF) of residues close to the ligand (within 5 Angstroms), highlighted in black, to assess their dynamic behavior within the binding pocket; (H) individual residue energy contributions from MMGBSA, pinpointing crucial stabilizers.

Elucidating the Stability of N7G within the SERPINE1 Active Site

Our analysis revealed that N7G is stably accommodated within the SERPINE1 active pocket, predominantly through non-polar interactions with hydrophobic residues. Across all triplicate (200 ns) trajectories, a consistent pattern of 17 non-polar interactions was observed involving residues Val39, Val42, Val140, Ile148, Leu151, Leu152, Ala156, Val164, Leu165, Val166, Ala168, Leu169, Leu286, Ala318, Ala320, Leu321, and Val324. Polar interactions also played a crucial role in stabilization, with Ser35, Thr144, Thr161, Asn167, Gln319, Gln322, and the positively charged Lys323 and Lys325 contributing to the stable occupancy of N7G. The formation of three to five hydrogen bonds with Ala156, Asn167, Leu321, Gln322, and Lys323 was instrumental in the stability of the N7G-SERPINE1 complex, as depicted in Figure 8A-C.

The 200 ns MD simulations confirmed that the SERPINE1-N7G complex maintained a stable backbone conformation with a root-mean-square deviation (RMSD) of 0.22 ± 0.02 nm (Figure 9 A). The ligand itself showed a stable RMSD ranging from 0.18 ± 0.03 to 0.3 ± 0.01 nm (Figure 9 B). The average minimum distance of 0.18 nm between N7G and SERPINE1 indicated the tight binding within the active site (Figure 9 C). A consistent radius of gyration (Rg) value between 2.15 ± 0.02 nm to 2.2 ± 0.03 nm across the simulations indicated a compact and stable complex formation (Figure 9 D). The complex was further characterized by an average of six to seven hydrogen bonds throughout the 200 ns simulations in runs 1, 2, and 3 (Figure 9 E), and a stable solvent accessible surface area between 170-185 nm² (Figure 9F). Analysis of the root-mean-square fluctuation (RMSF) of the active pocket residues revealed minimal fluctuations, signifying a stable interaction with N7G (Figure 9 G).

The MMGBSA analysis supported these observations with reliable binding free energies of -57.7694 ± 3.8023 kcal/mol, -61.0155 ± 4.3545 kcal/mol, and -61.2195 ± 3.7082 kcal/mol for runs 1, 2, and 3, respectively (Table 3). Residue decomposition analysis pinpointed Asn167 as the primary contributor to the stability of the SERPINE1-N7G complex (Figure 9 H). Other residues such as Leu151, Val166, Val164, Val42, Leu169, Val140, and Val148 also played significant roles in N7G binding, as shown in Figure 9 H.

The 200ns trajectory analysis revealed transient complex formation of N7G with MMP1 (Figure 10 A and B). N7G was initially bound to the pocket of the MMP1 protein but after a simulation time ~ 80 ns the complex was destabilized and the ligand was ejected out of the protein. The high fluctuations in the RMSD of the ligand with respect to the protein's backbone and the minimum distance between N7G and active site of MMP1, confirmed the destabilization of the complex (Figure 10 C and D).

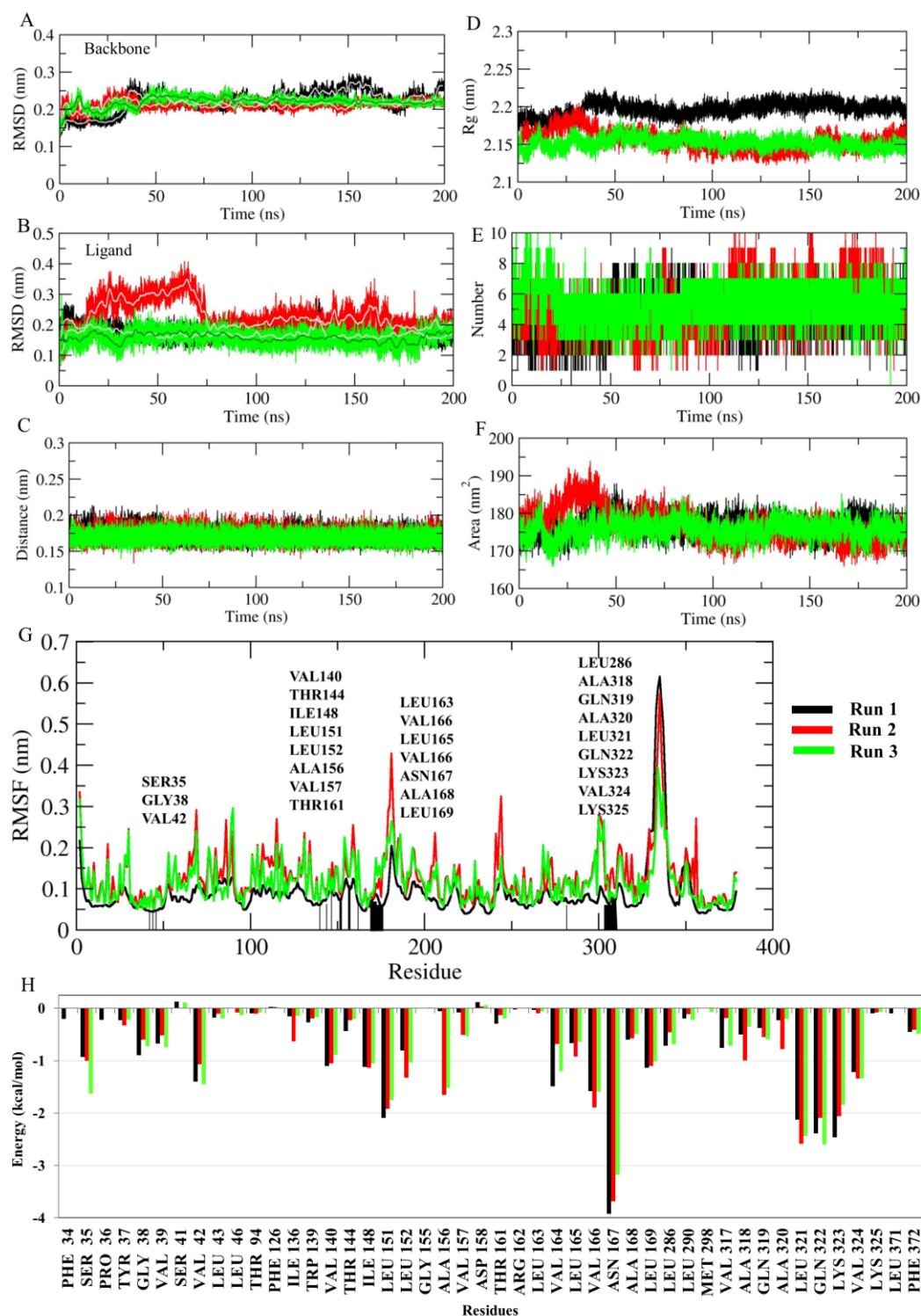


Figure 9: Molecular Dynamics Insights of SERPINE1-N7G Interaction. Illustrated are (A) protein backbone RMSD, indicating structural steadiness; (B) ligand N7G RMSD, showing binding stability; (C) ligand-protein proximity; (D) complex compactness via radius of gyration; (E) hydrogen bond frequency, affirming interaction strength; (F) solvent exposure through Solvent Accessible Surface Area; (G) binding site residue stability via RMSF, with key residues marked in black; and (H) individual residue energy contributions from MMGBSA.

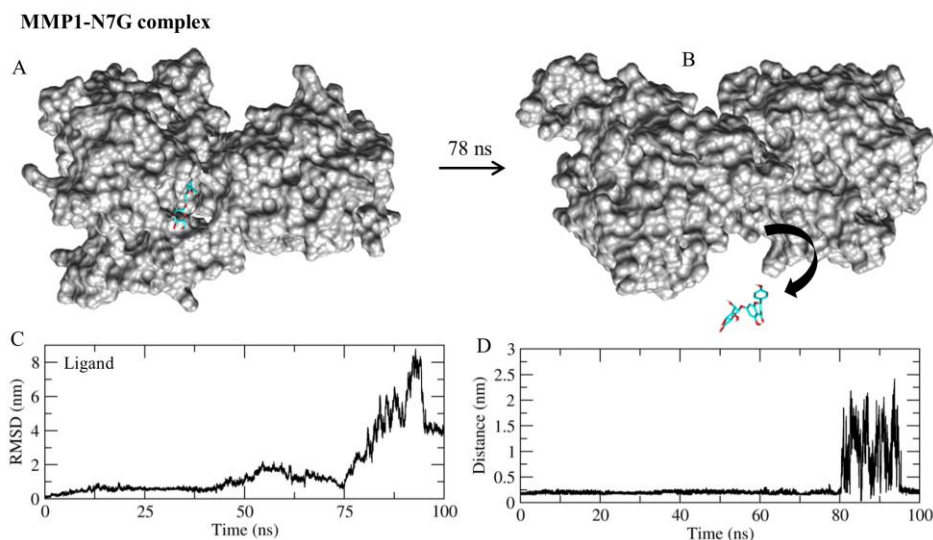


Figure 10: Trajectory Analysis of N7G with MMP1. (A) Shows the initial stable binding of N7G within MMP1's active pocket, while (B) illustrates the complex destabilization and ejection of N7G.

Table 3: Free energy calculations of N7G binding with host target proteins

Target-N7G complex		Energy Components						
		ΔE_{VDW}	ΔE_{EEL}	ΔE_{GB}	ΔE_{SURF}	ΔG_{gas}	ΔG_{solv}	ΔG_{TOTAL}
MMP7 (PDB ID: 2Y6D)	Run 1	-50.4860 \pm 5.6145	-23.7502 \pm 8.9262	38.8374 \pm 7.7013	-6.1440 \pm 0.4817	-74.2362 \pm 10.3413	32.6934 \pm 7.4466	-41.5428 \pm 4.7443
	Run 2	-52.9088 \pm 3.1746	-25.6410 \pm 6.7643	38.7198 \pm 5.0561	-6.3321 \pm 0.3248	-78.5497 \pm 7.3532	32.3877 \pm 4.9223	-46.1620 \pm 4.0393
	Run 3	-47.2523 \pm 2.6910	-19.1631 \pm 7.5603	37.6186 \pm 6.2523	-5.4614 \pm 0.2442	-66.4154 \pm 8.0981	32.1572 \pm 6.1835	-34.2582 \pm 3.7192
SERPINE1 (PDB ID: 1A7C)	Run 1	-60.1787 \pm 2.7485	-28.3364 \pm 6.3675	38.5826 \pm 4.0496	-7.8368 \pm 0.1241	-88.5151 \pm 5.9449	30.7457 \pm 4.0580	-57.7694 \pm 3.8023
	Run 2	-55.6126 \pm 3.162	-40.8565 \pm 7.2501	43.5042 \pm 4.3910	-8.0506 \pm 0.1481	-96.4691 \pm 6.7109	35.4536 \pm 4.3645	-61.0155 \pm 4.3545
	Run 3	-58.0844 \pm 3.1798	-32.4775 \pm 4.7790	37.3655 \pm 2.8157	-8.0230 \pm 0.1522	-90.5620 \pm 4.4782	29.3425 \pm 2.7952	-61.2195 \pm 3.7082

All energies are in **Kcal/mol** along with their standard deviation in parenthesis. ΔE_{VDW} : van der Waals contribution from MM; ΔE_{EEL} : electrostatic energy as calculated by the MM force field; ΔE_{GB} : the electrostatic contribution to the solvation free energy calculated by GB; ΔE_{SURF} : solvent-accessible surface area; ΔG_{gas} : gas-phase interaction energy; ΔG_{solv} : solvation free energy; ΔG_{TOTAL} : total binding free energy.

Discussion

In this study, we explored the therapeutic potential of Naringenin-7-O-glucoside (N7G), also known as Prunin, a bioactive flavone glycoside. N7G is recognized for its antiviral, antibacterial, antimalarial, and anticancer properties [50]. We focused on N7G's application in treating COVID-19, analyzing lung samples from both deceased and healthy SARS-CoV-2 infected patients [28, 29] to understand the molecular mechanisms and identify potential targets for therapeutic intervention.

Our enrichment analysis, focusing on the biological functions and pathways associated with Naringenin-7-O-glucoside (N7G) targets, has revealed their connection to metalloendopeptidase activity and protease binding. These pathways play critical roles in immune responses, and cellular signaling. Notably, our analysis highlights the importance of the HIF-1, AGE-RAGE, and IL-17 signaling pathways, all of which are known to contribute to the pathogenesis of diseases, including COVID-19, suggesting their potential as targets for therapeutic intervention. Our analysis indicates that suppressing the HIF-1 signaling pathway could mitigate lung inflammation associated with SARS-CoV-2 infection [51, 52]. The AGE-RAGE signaling pathway, known for its role in oxidative stress response, leads to cytokine production and subsequent trigger in inflammation. Targeting and blocking the AGE-RAGE pathway emerges as a promising strategy in treating COVID-19 [53-55]. Additionally, IL-17, a cytokine implicated in the cytokine storm observed during SARS-CoV-2 infection, presents itself as another potential therapeutic target. Several studies have suggested that modulating the IL-17 signaling pathway could be effective in developing treatments for COVID-19 [56-58]. Moreover, our research suggests targeting the relaxin signaling pathway, known for its ability to suppress inflammation and fibrosis, could be beneficial. This pathway has been identified as a potential therapeutic target in cardiovascular diseases and other inflammation-related conditions, adding another dimension to the potential applications of N7G in treating post-COVID-19 syndrome or 'long-haul COVID' and other diseases [59, 60].

We concentrated on identifying influential and druggable host genes to address SARS-CoV-2 infection, leading to the prioritization of three N7G drug targets: SERPINE1, MMP7, and MMP1. Both our study's results and corroborating evidence from the literature emphasize the crucial role of these genes in SARS-CoV-2 infection, highlighting the urgency to develop

therapies targeting them. Elevated levels of SERPINE1 in plasma and pulmonary edema fluid have been previously identified as indicators of early mortality risk in COVID-19 patients [61]. Additionally, our enrichment analysis revealed a role for SERPINE1 in the process of platelet degranulation. This aligns with previous findings in severe COVID-19 cases, where patients exhibited increased fibrin deposition in lung tissues due to impaired fibrinolysis [62]. The upregulation of SERPINE1 is reported to inhibit fibrinolysis, leading to platelet exhaustion and subsequent imbalances in clotting, which can result in thrombocytopenia [61, 63, 64]. Intriguingly, increased SERPINE1 expression in SARS-CoV-2 infected samples was associated with altered immune and inflammatory profiles compared to normal samples [65, 66]. This observation suggests a significant impact of SERPINE1 on the immune response in severe COVID-19 cases [67]. Given these findings, we propose that SERPINE1 could be a viable therapeutic target for N7G, particularly in addressing the excessive inflammation observed in severe cases of COVID-19. This potential for therapeutic intervention underscores the importance of further research into the role of SERPINE1 in COVID-19 pathology and treatment strategies.

Our study also highlights the significance of MMP1 and MMP7 as critical targets of Naringenin-7-O-glucoside (N7G). Matrix metalloproteinases (MMPs) are key enzymes that regulate tissue and organ homeostasis, and are used as potential biomarkers of COVID-19 severity [68-72]. Existing literature indicates that overexpression of MMPs can disturb the balance of the extracellular matrix, leading to tissue damage when their expression becomes pathologically elevated [73-76]. Specifically, the MMP1 gene has been linked to the severity of COVID-19, identified as a significantly elevated inflammatory factor in hospitalized patients compared to those with milder symptoms or healthy controls [70, 73, 77]. It is evident from the literature that viral load triggers an exaggerated immune response, including the expression and proteolytic activation of MMPs [73, 78, 79]. Matrix Metalloproteinases, including MMP1, MMP2, MMP7, MMP8, and MMP14, have been implicated in causing pulmonary edema by releasing chemokines and pro-inflammatory markers, making them potential biomarkers for assessing the severity of COVID-19 [75, 80, 81]. These results highlight the significance of MMP1 and MMP7 as potential therapeutic targets in treating COVID-19, especially considering their influence on immune response and tissue integrity. This is particularly relevant in the context of N7G targeting these enzymes. A deeper understanding of how N7G influences the regulation and

activity of these matrix metalloproteinases could offer valuable insights into managing and mitigating the severe impacts associated with COVID-19 infection.

The notable correlations between the targets of N7G and various respiratory ailments highlight the possible impact of genes such as SERPINE1, MMP7, and MMP1 on lung disease mechanisms. Specifically, their strong association with Idiopathic Pulmonary Fibrosis suggests their involvement in fibrotic processes, and their link to asthma indicates a role in inflammation and airway remodeling. Additionally, the presence of these genes in various lung cancers points to their potential contribution to cancer development. These insights offer a promising direction for future research aimed at unraveling the molecular pathways at play, thereby facilitating the development of new treatment approaches and early detection methods for respiratory conditions.

To assess and validate the inhibitory capabilities of N7G against SERPINE1, MMP1 and MMP7 these targets, we employed molecular docking techniques followed by extensive molecular dynamics (MD) simulations, each lasting 200 nanoseconds (ns) and conducted in triplicates. Our findings revealed that MMP7 and SERPINE1 formed stable complexes with N7G. Notably, N7G consistently occupied the zinc binding catalytic site of MMP7 across all MD simulations, showing interaction patterns similar to other known MMP7 inhibitors [48, 49]. For SERPINE1 [82, 83], N7G tightly bound to the inhibitor site, indicating a strong interaction.

The MMGBSA analysis of the MMP7-N7G and SERPINE1-N7G complexes confirmed their stability, with average binding affinities of -40.6543 ± 4.1676 kcal/mol and -60.0014 ± 3.955 kcal/mol, respectively. These results suggest that N7G could effectively inhibit both MMP7 and SERPINE1.

Although Naringenin-7-O-glucoside (N7G) showed transient complex formation with MMP1 in our molecular simulation studies, the role of MMP1 in the pathogenesis of COVID-19 cannot be overlooked. Elevated levels of MMP1 have been associated with increased inflammatory response in COVID-19 patients, indicating its potential as a biomarker and a target for therapeutic intervention [70, 73, 77]. Further research into the interaction between N7G and MMP1 could provide deeper insights into developing effective treatments for COVID-19, particularly in cases with severe lung involvement.

In conclusion, our study reveals MMP7, MMP1, and SERPINE1 as critical immune-related targets of N7G in combating SARS-CoV-2, positioning N7G as a potential novel inhibitor for treating COVID-19-induced lung inflammation and post-COVID-19 syndrome' or 'long-haul COVID. While these findings are promising, they mark only the initial steps in understanding N7G's therapeutic potential. Further in-vivo studies and comprehensive clinical trials are essential to establish N7G's safety and effectiveness in COVID-19 treatment. This study contributes to the growing body of knowledge on using natural compounds in antiviral treatments, opening new avenues for exploring the potential of N7G against various viral infections. Amid the global fight against COVID-19, our study emphasizes the need for exploring a range of therapeutic solutions, including natural products, in the quest for effective treatments.

Declaration of competing interest

The authors declare that there are no conflicts of interest with the contents of this article.

Author contributions statement

V.M and S.A. performed the computational experiments, literature survey and prepared the illustrations. D. conducted collected literature survey related to Naringenin-7-O-glucoside. MD simulations, energy calculations and analysis were performed by S.A. V.M and E.P. S.A. V.M. E.P. and RM analyzed data. R.M conceived, designed, wrote and supervised the whole study of the research.

Acknowledgments

Vibha Mishra and Divya are supported by Research Fellowship from the BHU. Shivangi Agrawal acknowledges the project assistant support from DST-CURIE. R.M. gratefully acknowledges the research support from DST-CURIE-2022-80, Govt. of India.

References

- [1] P. Mathur, S. Kottlil, Immunomodulatory therapies for COVID-19, *Frontiers in Medicine*, 9 (2022) 921452.
- [2] S.R. Bonam, S.V. Kaveri, A. Sakuntabhai, L. Gilardin, J. Bayry, Adjunct immunotherapies for the management of severely ill COVID-19 patients, *Cell Reports Medicine*, 1 (2020) 100016.
- [3] J. Alijotas-Reig, E. Esteve-Valverde, C. Belizna, A. Selva-O'Callaghan, J. Pardos-Gea, A. Quintana, A. Mekinian, A. Anunciacion-Llunell, F. Miró-Mur, Immunomodulatory therapy for the management of severe COVID-19. Beyond the anti-viral therapy: A comprehensive review, *Autoimmunity reviews*, 19 (2020) 102569.
- [4] S. Agrawal, E. Pathak, R. Mishra, V. Mishra, A. Parveen, S.K. Mishra, P.S. Byadgi, S. Dubey, A.K. Chaudhary, V. Singh, Computational exploration of the dual role of the phytochemical fortunellin: Antiviral activities against SARS-CoV-2 and immunomodulatory abilities against the host, *Computers in Biology and Medicine*, (2022) 106049.
- [5] A.S. Oseran, Y. Song, J. Xu, I.J. Dahabreh, R.K. Wadhera, J.A. De Lemos, S.R. Das, T. Sun, R.W. Yeh, D.S. Kazi, Long term risk of death and readmission after hospital admission with covid-19 among older adults: retrospective cohort study, *bmj*, 382 (2023).
- [6] Y. Xie, T. Choi, Z. Al-Aly, Long-term outcomes following hospital admission for COVID-19 versus seasonal influenza: a cohort study, *The Lancet Infectious Diseases*, (2023).
- [7] J.M. Flynn, Q.Y.J. Huang, S.N. Zvornicanin, G. Schneider-Nachum, A.M. Shaqra, N.K. Yilmaz, S.A. Moquin, D. Dovala, C.A. Schiffer, D.N. Bolon, Systematic analyses of the resistance potential of drugs targeting SARS-CoV-2 main protease, *ACS Infectious Diseases*, 9 (2023) 1372-1386.
- [8] W.H. Ng, P.C.H. Tang, S. Mahalingam, X. Liu, Repurposing of drugs targeting the cytokine storm induced by SARS-CoV-2, *British Journal of Pharmacology*, 180 (2023) 133-143.
- [9] Q. Wang, Y. Guo, L. Liu, L.T. Schwanz, Z. Li, M.S. Nair, J. Ho, R.M. Zhang, S. Iketani, J. Yu, Antigenicity and receptor affinity of SARS-CoV-2 BA. 2.86 spike, *Nature*, (2023) 1-3.
- [10] S. Yang, Y. Yu, Y. Xu, F. Jian, W. Song, A. Yisimayi, P. Wang, J. Wang, J. Liu, L. Yu, Fast evolution of SARS-CoV-2 BA. 2.86 to JN. 1 under heavy immune pressure, *The Lancet Infectious Diseases*, (2023).
- [11] J. Castillo, O. Benavente, J.A. del Rio, Hesperetin 7-O-glucoside and prunin in Citrus species (*C. aurantium* and *C. paradisi*). A study of their quantitative distribution in immature fruits and as immediate precursors of neohesperidin and naringin in *Citrus aurantium*, *Journal of Agricultural and Food Chemistry*, 41 (1993) 1920-1924.
- [12] X. Han, S. Gao, Y. Cheng, Y. Sun, W. Liu, L. Tang, D. Ren, Protective effect of naringenin-7-O-glucoside against oxidative stress induced by doxorubicin in H9c2 cardiomyocytes, *Bioscience Trends*, 6 (2012) 19-25.
- [13] X. Han, D. Ren, P. Fan, T. Shen, H. Lou, Protective effects of naringenin-7-O-glucoside on doxorubicin-induced apoptosis in H9C2 cells, *European Journal of Pharmacology*, 581 (2008) 47-53.
- [14] J. Achika, R. Ayo, A. Oyewale, J. Habila, Flavonoids with antibacterial and antioxidant potentials from the stem bark of *Uapaca heudelotti*, *Heliyon*, 6 (2020).
- [15] S. Wijaya, K.T. Jin, T.K. Nee, C. Wiart, In vitro 5-LOX inhibitory and antioxidant activities of extracts and compounds from the aerial parts of *Lopholaena coriifolia* (Sond.) E. Phillips & CA Sm, *Journal of Complementary and Integrative Medicine* 9(2012).

- [16] M. Li, W. Huang, F. Jie, M. Wang, Y. Zhong, Q. Chen, B. Lu, Discovery of Keap1– Nrf2 small– molecule inhibitors from phytochemicals based on molecular docking, *Food and Chemical Toxicology*, 133 (2019) 110758.
- [17] A. Nishina, D. Sato, J. Yamamoto, K. Kobayashi-Hattori, Y. Hirai, H. Kimura, Antidiabetic-like effects of Naringenin-7-O-glucoside from Edible Chrysanthemum ‘Kotobuki’ and Naringenin by Activation of the PI3K/Akt Pathway and PPAR γ , *Chemistry & Biodiversity*, 16 (2019) e1800434.
- [18] H.A. Jung, M.Y. Ali, H.K. Bhakta, B.-S. Min, J.S. Choi, Prunin is a highly potent flavonoid from *Prunus davidiana* stems that inhibits protein tyrosine phosphatase 1B and stimulates glucose uptake in insulin-resistant HepG2 cells, *Archives of pharmacal research*, 40 (2017) 37-48.
- [19] E.E. Eltamany, M.S. Nafie, D.M. Khodeer, A.H. El-Tanahy, M.S. Abdel-Kader, J.M. Badr, R.F. Abdelhameed, *Rubia tinctorum* root extracts: Chemical profile and management of type II diabetes mellitus, *RSC advances*, 10 (2020) 24159-24168.
- [20] J.S. Choi, T. Yokozawa, H. Oura, Antihyperlipidemic effect of flavonoids from *Prunus davidiana*, *Journal of natural products*, 54 (1991) 218-224.
- [21] X. He, Q. He, L. Sun, Protective Effect of Naringenin-7-O-glucoside in Carbon Tetra Chloride (CCl₄) Induced Hepatotoxicity in Rats: In Vitro and In Vivo Study, *LATIN AMERICAN JOURNAL OF PHARMACY*, 42 (2023) 481-488.
- [22] M.K. El-Ashrey, F. Elshibani, A. Alamami, N. Elremali, M.A. Elderbi, Prediction of Sars-Cov-2 Main Protease Potential Inhibitors from Libyan *Arbutus Pavarii* Pampan Compounds: A Molecular Docking Study, *Journal of Scientific and Innovative Research* 9(2020) 90-96.
- [23] N. Singh, P.P. Singh, Structure-Based Virtual Screening of Phytochemicals from *Phyllanthus Amarus* as Potent Inhibitory Phytochemicals Against Marburg Virus Disease, *receptor*, 8 (2023) 9.
- [24] M. Wurtele, C. Coelho, G. Gallo, C. Campos, L. Hardy, Y. Perez Castillo, M. Moriwaki, M.P. Kapoor, D.P. de Sousa, Inhibition of the SARS-CoV-2 Main Protease by Isoquercitrin γ -Cyclodextrin Inclusion Complex Formulations: A Biochemical and In Silico Study, *Journal of Chemistry*, 2023 (2023).
- [25] S.S. El-Hawary, M.Y. Issa, H.S. Ebrahim, A.F. Mohammed, A.M. Hayallah, E.M.A. El-Kader, A.M. Sayed, U.R. Abdelmohsen, Potential of (Citrus nobilis Lour \times Citrus deliciosa Tenora) metabolites on COVID-19 virus main protease supported by in silico analysis, *Natural Product Research*, 36 (2022) 2843-2847.
- [26] D. Gfeller, A. Grosdidier, M. Wirth, A. Daina, O. Michielin, V. Zoete, SwissTargetPrediction: a web server for target prediction of bioactive small molecules, *Nucleic acids research*, 42 (2014) W32-W38.
- [27] M.J. Keiser, B.L. Roth, B.N. Armbruster, P. Ernsberger, J.J. Irwin, B.K. Shoichet, Relating protein pharmacology by ligand chemistry, *Nature biotechnology*, 25 (2007) 197-206.
- [28] I. Papatheodorou, P. Moreno, J. Manning, A.M.-P. Fuentes, N. George, S. Fexova, N.A. Fonseca, A. Füllgrabe, M. Green, N. Huang, Expression Atlas update: from tissues to single cells, *Nucleic acids research*, 48 (2020) D77-D83.
- [29] M. Wu, Y. Chen, H. Xia, C. Wang, C.Y. Tan, X. Cai, Y. Liu, F. Ji, P. Xiong, R. Liu, Transcriptional and proteomic insights into the host response in fatal COVID-19 cases, *Proceedings of the National Academy of Sciences*, 117 (2020) 28336-28343.
- [30] G.D. Bader, C.W. Hogue, An automated method for finding molecular complexes in large protein interaction networks, *BMC bioinformatics*, 4 (2003) 1-27.

- [31] M.V. Kuleshov, M.R. Jones, A.D. Rouillard, N.F. Fernandez, Q. Duan, Z. Wang, S. Koplev, S.L. Jenkins, K.M. Jagodnik, A. Lachmann, Enrichr: a comprehensive gene set enrichment analysis web server 2016 update, *Nucleic acids research*, 44 (2016) W90-W97.
- [32] M. Kanehisa, S. Goto, KEGG: kyoto encyclopedia of genes and genomes, *Nucleic acids research*, 28 (2000) 27-30.
- [33] H. Wickham, ggplot2, *Wiley interdisciplinary reviews: computational statistics*, 3 (2011) 180-185.
- [34] J. Eberhardt, D. Santos-Martins, A.F. Tillack, S. Forli, AutoDock Vina 1.2. 0: New docking methods, expanded force field, and python bindings, *Journal of Chemical Information and Modeling*, 61 (2021) 3891-3898.
- [35] H.M. Berman, J. Westbrook, Z. Feng, G. Gilliland, T.N. Bhat, H. Weissig, I.N. Shindyalov, P.E. Bourne, The protein data bank, *Nucleic acids research*, 28 (2000) 235-242.
- [36] G.M. Morris, R. Huey, W. Lindstrom, M.F. Sanner, R.K. Belew, D.S. Goodsell, A. Olson, AutoDock4 and AutoDockTools4: Automated docking with selective receptor flexibility, *Journal of computational chemistry*, 30 (2009) 2785-2791.
- [37] E.F. Pettersen, T.D. Goddard, C.C. Huang, G.S. Couch, D.M. Greenblatt, E.C. Meng, T.E. Ferrin, UCSF Chimera—a visualization system for exploratory research and analysis, *Journal of computational chemistry*, 25 (2004) 1605-1612.
- [38] M.J. Abraham, T. Murtola, R. Schulz, S. Páll, J.C. Smith, B. Hess, E.J.S. Lindahl, GROMACS: High performance molecular simulations through multi-level parallelism from laptops to supercomputers, *SoftwareX*, 1-2 (2015) 19-25.
- [39] J. Huang, S. Rauscher, G. Nawrocki, T. Ran, M. Feig, B.L. De Groot, H. Grubmüller, A.D. MacKerell, CHARMM36m: an improved force field for folded and intrinsically disordered proteins, *Nature methods*, 14 (2017) 71-73.
- [40] V. Zoete, M.A. Cuendet, A. Grosdidier, O. Michielin, SwissParam: a fast force field generation tool for small organic molecules, *Journal of computational chemistry*, 32 (2011) 2359-2368.
- [41] G. Bussi, D. Donadio, M. Parrinello, Canonical sampling through velocity rescaling, *The Journal of chemical physics*, 126 (2007) 014101.
- [42] M. Parrinello, A. Rahman, Polymorphic transitions in single crystals: A new molecular dynamics method, *Journal of Applied physics*, 52 (1981) 7182-7190.
- [43] T. Darden, D. York, L. Pedersen, Particle mesh Ewald: An $N \cdot \log(N)$ method for Ewald sums in large systems, *The Journal of chemical physics*, 98 (1993) 10089-10092.
- [44] B. Hess, H. Bekker, H.J. Berendsen, J.G. Fraaije, LINCS: a linear constraint solver for molecular simulations, *Journal of computational chemistry*, 18 (1997) 1463-1472.
- [45] D.A. Case, H.M. Aktulga, K. Belfon, I. Ben-Shalom, S.R. Brozell, D. Cerutti, T. Cheatham, V.W.D. Cruzeiro, T. Darden, R.E. Duke, Amber 2021: Reference Manual, (2021).
- [46] B.R. Miller III, T.D. McGee Jr, J.M. Swails, N. Homeyer, H. Gohlke, A.E. Roitberg, MMPBSA.py: an efficient program for end-state free energy calculations, *Journal of chemical theory computation*, 8 (2012) 3314-3321.
- [47] M.S. Valdés-Tresanco, M.E. Valdés-Tresanco, P.A. Valiente, E. Moreno, gmx_MMPBSA: a new tool to perform end-state free energy calculations with GROMACS, *Journal of Chemical Theory and Computation*, 17 (2021) 6281-6291.
- [48] F. Meng, H. Yang, C. Jack, H. Zhang, A. Moller, D. Spivey, R.C. Page, D.L. Tierney, M.W. Crowder, Biochemical characterization and zinc binding group (ZBGs) inhibition studies on the catalytic domain of MMP7 (cdMMP7), *Journal of Inorganic Biochemistry*, 165 (2016) 7-17.

- [49] S. Molière, A. Jaulin, C.-L. Tomasetto, N. Dali-Youcef, Roles of Matrix Metalloproteinases and Their Natural Inhibitors in Metabolism: Insights into Health and Disease, *International Journal of Molecular Sciences*, 24 (2023) 10649.
- [50] F. Yarmohammadi, R. Rezaee, G. Karimi, Natural compounds against doxorubicin-induced cardiotoxicity: a review on the involvement of Nrf2/ARE signaling pathway, *Phytotherapy Research*, 35 (2021) 1163-1175.
- [51] M. Jahani, S. Dokaneheifard, K. Mansouri, Hypoxia: A key feature of COVID-19 launching activation of HIF-1 and cytokine storm, *Journal of inflammation*, 17 (2020) 1-10.
- [52] E. Ferraro, M. Germanò, R. Mollace, V. Mollace, N. Malara, HIF-1, the Warburg effect, and macrophage/microglia polarization potential role in COVID-19 pathogenesis, *Oxidative Medicine and Cellular Longevity*, 2021 (2021).
- [53] N. Berntsen, B. Fosby, C. Tan, H. Reims, J. Ogaard, X. Jiang, E. Schrupf, L. Valestrand, T. Karlsen, P.-D. Line, Natural killer T cells mediate inflammation in the bile ducts, *Mucosal immunology*, 11 (2018) 1582-1590.
- [54] R. Ramasamy, S.F. Yan, A.M. Schmidt, Receptor for AGE (RAGE): signaling mechanisms in the pathogenesis of diabetes and its complications, *Annals of the New York Academy of Sciences*, 1243 (2011) 88-102.
- [55] D. Sellegounder, P. Zafari, M. Rajabinejad, M. Taghadosi, P. Kapahi, Advanced glycation end products (AGEs) and its receptor, RAGE, modulate age-dependent COVID-19 morbidity and mortality. A review and hypothesis, *International immunopharmacology*, 98 (2021) 107806.
- [56] T. Shibabaw, Inflammatory cytokine: IL-17A signaling pathway in patients present with COVID-19 and current treatment strategy, *Journal of inflammation research*, (2020) 673-680.
- [57] X. Lin, B. Fu, S. Yin, Z. Li, H. Liu, H. Zhang, N. Xing, Y. Wang, W. Xue, Y. Xiong, ORF8 contributes to cytokine storm during SARS-CoV-2 infection by activating IL-17 pathway, *Iscience*, 24 (2021).
- [58] V. Bulat, M. Situm, M.D. Azdajic, R. Likic, Potential role of IL-17 blocking agents in the treatment of severe COVID-19?, *British Journal of Clinical Pharmacology*, 87 (2021) 1578.
- [59] B. Martin, B.A. Gabris-Weber, R. Reddy, G. Romero, A. Chattopadhyay, G. Salama, Relaxin reverses inflammatory and immune signals in aged hearts, *PloS one*, 13 (2018) e0190935.
- [60] S. Mehandru, M. Merad, Pathological sequelae of long-haul COVID, *Nature immunology*, 23 (2022) 194-202.
- [61] Y. Zuo, M. Warnock, A. Harbaugh, S. Yalavarthi, K. Gockman, M. Zuo, J.A. Madison, J.S. Knight, Y. Kanthi, D.A. Lawrence, Plasma tissue plasminogen activator and plasminogen activator inhibitor-1 in hospitalized COVID-19 patients, *Scientific reports*, 11 (2021) 1580.
- [62] C. Nougier, R. Benoit, M. Simon, H. Desmurs-Clavel, G. Marcotte, L. Argaud, J.S. David, A. Bonnet, C. Negrier, Y. Dargaud, Hypofibrinolytic state and high thrombin generation may play a major role in SARS-COV2 associated thrombosis, *Journal of Thrombosis and Haemostasis*, 18 (2020) 2215-2219.
- [63] M.M. Lamers, B.L. Haagmans, SARS-CoV-2 pathogenesis, *Nature reviews microbiology*, 20 (2022) 270-284.
- [64] N. Mackman, S. Antoniak, A.S. Wolberg, R. Kasthuri, N.S. Key, Coagulation abnormalities and thrombosis in patients infected with SARS-CoV-2 and other pandemic viruses, *Arteriosclerosis, Thrombosis, and Vascular Biology*, 40 (2020) 2033-2044.

- [65] M. Roussel, J. Ferrant, F. Reizine, S. Le Gallou, J. Dulong, S. Carl, M. Lesouhaitier, M. Gregoire, N. Bescher, C. Verdy, Comparative immune profiling of acute respiratory distress syndrome patients with or without SARS-CoV-2 infection, *Cell Reports Medicine*, 2 (2021).
- [66] J.-Y. Zhang, J.P. Whalley, J.C. Knight, L.S. Wicker, J.A. Todd, R.C. Ferreira, SARS-CoV-2 infection induces a long-lived pro-inflammatory transcriptional profile, *Genome Medicine*, 15 (2023) 1-12.
- [67] T.F. Kellici, E.S. Pilka, M.J. Bodkin, Therapeutic potential of targeting plasminogen activator inhibitor-1 in COVID-19, *Trends in Pharmacological Sciences*, 42 (2021) 431-433.
- [68] H. Laronha, J. Caldeira, Structure and function of human matrix metalloproteinases, *Cells*, 9 (2020) 1076.
- [69] U. Khalid, D. Dimov, T.J.B. Vlaykova, B. Equipment, Matrix metalloproteinases in COVID-19: underlying significance, 37 (2023) 295-301.
- [70] M.A. Zingaropoli, T. Latronico, P. Pasculli, G.M. Masci, R. Merz, F. Ciccone, F. Dominelli, C. Del Borgo, M. Lichtner, F.J.B. Iafrate, Tissue Inhibitor of Matrix Metalloproteinases-1 (TIMP-1) and Pulmonary Involvement in COVID-19 Pneumonia, 13 (2023) 1040.
- [71] M. Gelzo, S. Cacciapuoti, B. Pinchera, A. De Rosa, G. Cerner, F. Scialò, M. Comegna, M. Mormile, G. Fabbrocini, R.J.S.R. Parrella, Matrix metalloproteinases (MMP) 3 and 9 as biomarkers of severity in COVID-19 patients, 12 (2022) 1212.
- [72] N. Pavan Kumar, A. Venkataraman, P. Varadarjan, A. Nancy, A. Rajamanickam, E. Selladurai, T. Sankaralingam, K. Thiruvengadam, R. Selvam, A.J.F.i.M. Thimmaiah, Role of matrix metalloproteinases in multi-system inflammatory syndrome and acute COVID-19 in children, 9 (2022) 1050804.
- [73] F. Syed, W. Li, R.F. Relich, P.M. Russell, S. Zhang, M.K. Zimmerman, Q. Yu, Excessive matrix metalloproteinase-1 and hyperactivation of endothelial cells occurred in COVID-19 patients and were associated with the severity of COVID-19, *The Journal of infectious diseases*, 224 (2021) 60-69.
- [74] Q. Ning, D. Wu, X. Wang, D. Xi, T. Chen, G. Chen, H. Wang, H. Lu, M. Wang, L.J.S.T. Zhu, T. Therapy, The mechanism underlying extrapulmonary complications of the coronavirus disease 2019 and its therapeutic implication, 7 (2022) 57.
- [75] R. Salomão, V. Assis, I.V. de Sousa Neto, B. Petriz, N. Babault, J.L.Q. Durigan, R.J.B. de Cássia Marqueti, Involvement of Matrix Metalloproteinases in COVID-19: Molecular Targets, Mechanisms, and Insights for Therapeutic Interventions, 12 (2023) 843.
- [76] S. Ramezani, F. Ezzatifar, T. Hojjatipour, M. Hemmatzadeh, A.G. Shabgah, J.G. Navashenaq, S. Aslani, N. Shomali, M. Arabi, F.J.M.B.R. Babaie, Association of the matrix metalloproteinases (MMPs) family gene polymorphisms and the risk of coronavirus disease 2019 (COVID-19); implications of contribution for development of neurological symptoms in the COVID-19 patients, 50 (2023) 173-183.
- [77] Y. Tuharov, D. Krenytska, T. Halenova, L. Kot, N. Raksha, O. Savchuk, L. Prysiazniuk, R. Matkivska, T. Falalyeyeva, L.J.R.o.R.C.T. Ostapchenko, Plasma Levels of MMPs and TIMP-1 in Patients with Osteoarthritis After Recovery from COVID-19, 18 (2023) 123-128.
- [78] B. Safont, J. Tarraso, E. Rodriguez-Borja, E. Fernández-Fabrellas, J.N. Sancho-Chust, V. Molina, C. Lopez-Ramirez, A. Lope-Martinez, L. Cabanes, A.L. Andreu, Lung function, radiological findings and biomarkers of fibrogenesis in a cohort of COVID-19 patients six months after hospital discharge, *Archivos de Bronconeumologia*, 58 (2022) 142-149.
- [79] J.-J. Huang, C.-W. Wang, Y. Liu, Y.-Y. Zhang, N.-B. Yang, Y.-C. Yu, Q. Jiang, Q.-F. Song, G.-Q.J.W.J.o.C.C. Qian, Role of the extracellular matrix in COVID-19, 11 (2023) 73.

- [80] U. Khalid, D. Dimov, T. Vlaykova, Matrix metalloproteinases in COVID-19: underlying significance, *Biotechnology and Biotechnological Equipment*, 37 (2023) 295-301.
- [81] S.L. Murphy, B. Halvorsen, J.C. Holter, C. Huse, A. Tveita, M. Trøseid, H. Hoel, A.B. Kildal, A.R. Holten, T.V. Lerum, Circulating markers of extracellular matrix remodelling in severe COVID-19 patients, *Journal of Internal Medicine*, (2023).
- [82] M. Sillen, T. Miyata, D.E. Vaughan, S.V. Strelkov, P.J. Declerck, Structural insight into the two-step mechanism of PAI-1 inhibition by small molecule TM5484, *International journal of molecular sciences*, 22 (2021) 1482.
- [83] K.A. Vousden, T. Lundqvist, B. Popovic, B. Naiman, A.M. Carruthers, P. Newton, D.J. Johnson, A. Pomowski, T. Wilkinson, P. Dufner, Discovery and characterisation of an antibody that selectively modulates the inhibitory activity of plasminogen activator inhibitor-1, *Scientific reports*, 9 (2019) 1605.